Carbon Capture and Usage by MXenes

Raul Morales-Salvador,[†,¶] José D. Gouveia,[‡,¶] Ángel Morales-García,[†] Francesc Viñes[*,†] José R. B. Gomes,[‡] Francesc Illas[†]

[†]*Departament de Ciència de Materials i Química Física & Institut de Química Teòrica i Computacional (IQTCUB), Universitat de Barcelona, c/ Martí i Franquès 1-11, 08028 Barcelona, Spain*

[‡]*CICECO – Aveiro Institute of Materials, Department of Chemistry, University of Aveiro, Campus Universitário de Santiago, Aveiro, Portugal*

[*] Corresponding author: Francesc Viñes (francesc.vines@ub.edu)

ABSTRACT

Two-dimensional (2D) pristine M_2X MXenes are proposed as highly active catalytic materials for carbon dioxide (CO_2) greenhouse gas conversion into carbon monoxide (CO) on the basis of a multiscale modeling approach, coupling calculations carried out in the framework of density functional theory and newly developed kinetic phase diagrams. The extremely facile CO_2 conversion into CO leaves the MXene surfaces partially covered by atomic oxygen, recovering its pristine nature by a posterior catalyst regeneration by hydrogen (H_2) treatment at high temperatures, MXenes effectively working as a two-step catalyst for the reverse water-gas shift reaction.

Keywords: MXenes, CO_2 utilization, heterogeneous catalysis, reverse water gas shift, density functional simulations, kinetic phase diagrams

[¶] Both authors equally contributed

1. Introduction

The ever-growing energy demands to sustain the current society wellness standards has put climate at stake, where one of the major causes of global warming is the anomalous high concentration of carbon dioxide (CO_2) greenhouse gas present in the atmosphere.[1] Actions are being taken to reduce the CO_2 emissions, *e.g.* exploiting clean energy sources, or even maximizing the energy profit from other existing ones. Still, exceedingly large amounts of CO_2 are and will be poured into the atmosphere, and complementary actions and processes are sought in order to mitigate the climate change.

Among several plausible technologies, carbon capture and storage (CCS)[2-4] has been highlighted to eliminate 550 billion CO_2 tons in the atmosphere, needed to return to the pre-industrial natural situation.[5] For CCS, materials are sought able to anchor CO_2 at standard conditions, a task challenged by the CO_2 high molecular stability and consequent low activity. More appealing than CCS are carbon capture and utilization (CCU) technologies,[6-8] aimed at using CO_2 as a C_1 chemical feedstock; by this, CO_2 can be chemically converted into other greener and potentially industrially-useful chemicals, such as methanol, currently used in fuel cells,[9] or carbon monoxide (CO), which can be later used in the Fischer-Tropsch process synthesizing C_n hydrocarbons.[10,11] The back-formation of re-usable fuels by CCU while using renewable sources of energy, and other sustainable reagents, *e.g.* hydrogen (H_2) from water photocatalysis, conforms a plausible path towards closing the C-cycle.

A *sine qua non* pre-requisite for CO_2 catalytic conversion is having a material able to capture it under reaction *operando* conditions. Besides, given the very high CO_2 stability, such a material would need to be able to activate it, which naturally implies a substrate→CO_2 charge transfer and the formation of a chemically active, bent $CO_2^{\delta-}$ moiety. Recently, two-dimensional (2D) transition metal carbides and nitrides, named MXenes,[12] have been proposed for CCS technologies based on estimates from density functional theory (DFT) calculations, meeting the aforementioned criteria while featuring very high gravimetric CO_2 loadings thanks to their intrinsic high surface areas.[13,14] Such a forecast mentioned has been recently experimentally confirmed on pristine Ti_3C_2 MXene, successfully reaching a very high CO_2 uptake of 12 $mol \cdot kg^{-1}$,[15] thus surpassing other previous values on other employed solid sorbents.[13]

Inspired by the promising performance in the electrocatalytic and photocatalytic[16] CO_2 reduction of a series of MXene-based compounds, including O-

and OH-terminated MXenes,[17-19] vacancy-containing MXenes,[20] and even MXene-based composites,[21] and spurred by the aforementioned CCS technology achievement, we show here compelling theoretical evidence, based on accurate DFT simulations and newly developed kinetic phase diagrams, of the very high CCU activity of the MXenes family, catalyzing the CO formation, a product that be subsequently used in methanol synthesis or introduced in Fischer-Tropsch plants to produce hydrocarbons. A further two-step procedure to catalyze the reverse water gas shift (RWGS) reaction —$CO_2 + H_2 \rightarrow CO + H_2O$— is presented based on existing experimental procedures for obtaining pristine MXene surfaces.[15] Note that very recent synthetic protocols permit synthetizing bare MXenes, making their usage further attractive for CCU activities.[22]

2. Methods and Models

A broad set of MXenes with M_2X formula has been studied, including transition metals (M) from groups IV (Ti, Zr, Hf), V (V, Nb, Ta), and VI (Cr, Mo, W), while X = C or N, totaling 18 M_2X (0001) surface systems, studied by means of surface slab models as done in previous studies.[13,14] These consist of *p*(3×3) supercells containing 18 metal and 9 C or 9 N atoms arranged in three atomic layers —*i.e.*, a sandwiched M_2X structure has been used. In all calculations, a full geometry optimization was considered where positions of MXene and adsorbates atoms were fully relaxed. The employed *p*(3×3) supercells slab models have a length of 16 Å along the (0001) unit cell vector, which ensures at least 10 Å of vacuum among the material replicas along the direction normal to the MXene surface, enough to avoid the interaction among the slabs or of the adsorbates with the replicated slabs, see Figure 1. This also ensures a low coverage regime of a sole CO_2, CO, or O moiety per every nine surface metal atoms.

The present DFT calculations were carried out using the periodic Vienna *ab initio* simulation package (VASP).[23] Following previous procedures on the interaction of CO_2 and MXenes, the Perdew-Burke-Ernzerhof (PBE) exchange-correlation functional,[24] combined with the Grimme D3 treatment of dispersive forces.[25] The PBE-D3 choice is supported by previous studies showing that it accurately predicts the interaction of CO_2 with MXenes and transition metal carbides (TMCs).[13,14,26,27] Projector augmented wave (PAW) pseudopotentials were used to describe the effect of core electrons onto the valence electron density.[28] The latter was expanded in a plane wave basis set with a cut-off energy of 415 eV. The Brillouin zone integration was

sampled using an optimal Monkhorst-Pack **k**-grid of a 5×5×1 dimensions.[29] The threshold for the electronic optimization was set to 10^{-5} eV, and geometry optimizations were considered finished when forces acting on atoms were below 0.01 eV $Å^{-1}$. During optimizations, the coordinates of all the atoms in the cell were allowed to fully relax. Test calculations using more stringent values for kinetic energy cutoff, the **k**-points mesh, or the thresholds used as optimization criteria yielded variations in the computed adsorption energies below chemical accuracy, *i.e.* below ~0.04 eV —1 kcal·mol^{-1}. The effect of spin polarization was considered as well and found to be significant for the Ti_2N and Ti_2C MXenes only, with reductions on the E_{ads} of at most 0.2-0.3 eV. However, this corresponds to a small fraction of E_{ads}, and consequently, spin polarization was safely disregarded in the oncoming discussion.

For each adsorbate (CO_2, CO, or O), four high symmetry sites were sampled, see Figure 1, including top (T), bridge (B), and two types of three-fold hollow sites, either with an X atom (H_x) or a metal (H_m) atom beneath. For CO_2 and CO, different molecular conformations —perpendicular, planar, or tilted— were also considered, and, for each, at least two different orientations with respect the MXene most stable (0001) surface were sampled. To distinguish among the different adsorption sites, a coordination chemistry-based notation is used, so η^n denotes the number *n* of atoms of the adsorbed species bound to the surface, followed by a string tagging such atoms. The μ^m term denotes how many *m* atoms of the surface are implicated in the adsorption of the species. Next, the position of the *n* atoms is specified, stating their location over a T (t), B (b), H_m (m), or H_x (x) site. For instance, an O atom adsorbed on a H_x site would be η^1-O-μ^3-O_x, although for commodity, only the last part is commonly stated (O_x), as sufficient for an unequivocal identification, see Tables S1-S5 and Figures S1 and S2 of Section S1 of the Supporting Information (SI).

The geometry optimization calculations, necessary to determine the minimum energy atomic structure of adsorbates, were performed by initially placing the different species ~2 Å above the MXene surface, and then fully relaxing all the structure as above indicated. The located minima were subsequently characterized *via* a vibrational analysis, performed through the building up and subsequent diagonalization of the block of the Hessian matrix corresponding to adsorbate degrees of freedom. The elements of the Hessian matrix were obtained from finite differences of analytical gradients with displacements of 0.03 Å. Note that, within this approach, the molecular vibrations are

considered decoupled from the MXene phonons. Nevertheless, test calculations including MXene phonons yielded marginal variations on the zero point energy (ZPE) contribution to the calculated adsorption energy values, below the aforementioned chemical accuracy of ~0.04 eV. Note also that the vibrational frequencies thus computed are obtained within the harmonic approximation.

The adsorption energy of each species, E_{ads}^{S}, are defined as:

$$E_{ads}^{S} = E_{S/MXene} - E_{MXene} - E_{S} + \Delta E_{ZPE} \quad (1),$$

where $E_{S/MXene}$ corresponds to the total energy of the adsorbed *S* species, namely, CO_2, CO, or O, on a MXene surface; E_{MXene} stands for the energy of the relaxed, bare MXene; and E_S corresponds to the energy of the isolated species, computed in an asymmetric box of 9×10×11 Å dimensions at **Γ**-point to force a correct orbital occupancy. The ΔE_{ZPE} term corresponds to the difference in ZPE of the species in gas phase or adsorbed. According to this E_{ads}^{S} definition, favorable adsorption is associated to negative values, and hence, the more negative the E_{ads}, the stronger the adsorption is.

Note that for linear isolated molecules in vacuum, such as CO and CO_2, the number of normal vibrations modes corresponds to 3*N*-5, where *N* is the number of atoms of the molecule. However, for a given adsorbed molecule, the linear symmetry is removed and the rotational and translation normal modes become frustrated due to the interactions among the adsorbate and the MXene substrate. Therefore, the formal number of normal vibrational modes of adsorbed species becomes always 3*N*. That considered, the ZPE for gas phase species or when adsorbed are calculated as:

$$E_{\mathrm{S,vac}}^{\mathrm{ZPE}} = \frac{1}{2}\sum_{i=1}^{3N-5} \hbar\omega_i \quad (2),$$

$$E_{\mathrm{S,ads}}^{\mathrm{ZPE}} = \frac{1}{2}\sum_{i=1}^{3N} \hbar\omega_i \quad (3),$$

where ħ is the reduced Planck constant, and ω_i are the vibrational frequencies. So, the ZPE term is simply:

$$\Delta E_{\mathrm{ZPE}} = E_{\mathrm{S,ads}}^{\mathrm{ZPE}} - E_{\mathrm{S,vac}}^{\mathrm{ZPE}} \quad (4).$$

The search for the transitions states (TSs) corresponding to CO_2 dissociation was carried out by means of either the climbing-image nudged elastic band (CI-NEB)

method,[30] the adaptive NEB (ANEB),[31] the dimer,[32] or the improved dimer methodologies.[33] The search of such TS was carried out departing from most stable adsorption configurations of CO_2, but other CO_2 adsorption minima close in energy were also regarded as initial structures.

3. Results and discussion

As far as the adsorptive landscapes are concerned, for the CO_2 adsorption landscape on M_2X (0001) surfaces we refer to the literature,[13,14,34] with the adsorption energy values, $E_{ads}^{CO_2}$, ranging from -1.22 (Mo_2N) to -3.65 eV (Ti_2C). For CO, the adsorption energy estimates, E_{ads}^{CO}, are between -2.21 (W_2C) and -3.37 eV (Ti_2C); see further details in Tables S1-S5 of Section S1 of the SI. The affinity of MXenes towards atomic O is rather large, with E_{ads}^{O} ranging from -7.03 (Mo_2C) to -9.02 eV (Hf_2N), in line with experimental observations on as-synthesized terminated MXenes,[12,15,35,36] and previous estimates.[37,38] Indeed, the very large E_{ads}^{O} has been argued to be a descriptor of the CO_2 splitting on TMCs, acting as a driving force towards CO_2 splitting.[39]

It is worth noticing that the local geometric and electronic structure of 2D M_2C (0001) surfaces resemble the highly-unstable, hard-to-prepare rocksalt TMC (111) surfaces, to the point that the TMC (111) surfaces reactivity compares to that of (0001) M_2C MXene surfaces, similarly as well to thicker MXenes such as M_3C_2 and M_4C_3.[40] On MXenes, the adsorption strength seems to be enhanced *i*) firstly by larger surface metal positive charge, ΔQ_m, evaluated through a Bader topological analysis of the electron density,[41,42] see Figure 2 and, as a consequence *ii*) the resulting larger *d*-band center, ε_d, as proposed by Hammer and Nørskov,[43] see Figure 3. In this context, the descriptor dependences for CO_2* and O* are found to be similar, while CO* features a more attenuated trend. Further details on the descriptors estimation, their values, and the linear adjustment are found in Tables S6 and S7, respectively, of Section S2 of the SI.

The mentioned large O* attachment strength favors the CO_2 splitting exothermicity, with reaction energy values, ΔE_r, ranging from -0.88 (Ta_2N) to -2.75 eV (Hf_2N), see Table 1. On the basis of the well-known Brønsted–Evans–Polanyi (BEP) relationships, one could venture low energy barriers for CO_2* splitting, E_b^{dis}. This is fully confirmed by the present E_b^{dis} estimates revealing an extremely easy CO_2 dissociation, going from essentially barrierless situations to, at most, quite tolerable

barriers of up to 0.54 eV (W_2C). At the same time, given the large reaction step exothermicity, this implies having large recombination —*i.e.* CO_2* formation— energy barriers, E_b^{rec}, see Table 1. Given the rich CO_2* adsorptive landscape, E_b^{dis} values were gained by departing from energetically competitive CO_2 adsorption conformations, unfolding negligible E_b^{dis} variations of *ca.* 0.03 eV in average terms. Once the CO_2* is dissociated, the resulting CO* and O* moieties could diffuse to more distant positions; the diffusion energy barriers, E_b^{dif}, range from 0.20 (Ti_2C) to 1.06 eV (Ta_2C), see Table S8 of Section S3 of the SI, implying, in certain cases, a site steadiness upon CO_2 breakage.

Furthermore, note that the presently studied E_b^{dis} are ~2 to *ca.* 130 times smaller than the value of 1.33 eV, as obtained with comparable PBE-D3 calculations on a Cu(111) surface slab model,[44] a suited model for the Cu/ZnO catalyst industrially used to produce methanol from syngas. Notice that lower E_b^{dis} of 0.67 eV are found on Cu(111) step sites, which seem to be key for the CO_2 dissociation. Aside, a previous joined computational and experimental study on partially oxidized Mo_2C(0001) surface seems to rule out the possible coke formation, as the CO dissociation energy barrier of 1.59 eV is found to be excessively high.[45]

Thus, the CO formation directly from CO_2 is highly promoted on M_2X MXenes, and likely to be met on other thicker M_3X_2 and M_4X_3 MXenes, known to display very similar CO_2 affinities.[40] Figure 4 shows the CO_2 dissociation reaction energy profile for the two limit M_2X situations with the strongest and weakest attachment of CO_2; Ti_2C and Mo_2N, respectively. Clearly, the reaction profile is maintained regardless of the situation under scrutiny, *albeit* with an energy shift of the reaction intermediates, with only small variations depending on the different CO_2 *vs.* CO adsorption strengths. Notice the very low CO_2 dissociation E_b^{dis} values of 0.14 eV for Ti_2C and below the chemical accuracy of 0.04 eV for Mo_2N. The reaction profiles for the rest of the studied M_2X MXenes are depicted in Figures S3-S5 of Section S4 of the SI.

The E_b^{dis} on Mo_2C MXene (0001) surface of 0.31 eV agrees with previous joined theoretical and experimental studies on partially oxidized Mo_2C of 0.31 eV —estimated at 800 ºC, *i.e.* ~1073 K, and a CO_2 partial pressure of 1 bar, *i.e.* 105 Pa, in perfect agreement with the present value of 0.30 eV when accounting for such operating conditions—,[45] and on the similar hexagonal α-Mo_2C Mo-terminated (0001) surface of 0.19 eV.[26] As observed on Figure 4 and other profiles, see Figures S3-S5 of Section S4

of the SI, the as-split neighboring adsorbed CO and O moieties generally feature steric and coulombic repulsions, which can be reduced when either O, CO, or both adsorbed moieties diffuse to reach distant positions. As above stated, the diffusion energy barriers, E_b^{dif}, can be very easily surmounted, as exemplified on Ti_2C, with a diffusion value of 0.20 eV, yet other values, see Table S8 of Section S3 of the SI, can be more scattered, up to 1.06 eV for O diffusion on Ta_2C. Regardless of the previous, the mild gain in energy by moiety diffusion barely affects the overall reaction landscape profile.

The previous analysis undoubtedly reveals the very high CO_2 capture and direct dissociating capabilities of the MXenes family. The final step of the catalyzed reaction is the desorption of the CO product. This is tackled on Figure 5 based on the kinetic phase diagrams extracted from the CO_2 and CO adsorption *vs.* desorption rate constant estimates, obtained by means of collision theory and transition state theory (TST) models, respectively. Details on the followed mathematical framework and the kinetic phase diagrams can be found in the discussion and Figures S6-S8 of Sections S5 and S6 of the SI, respectively, as well as details can be gained from different sources of the literature.[13,27,40]

Two different types of reacting behavior can be found on MXenes, exemplified in the kinetic phase diagrams of Ti_2C and Mo_2N in Figure 5. On Ti_2C, operating conditions involving higher pressures and lower temperatures than the CO_2 adsorption/desorption equilibrium (black) line would lead to having CO* and O* present at the surface. For the CO* product to be released, one should increase the temperature and decrease the CO partial pressure so as to cross the CO adsorption/desorption equilibrium (red) line. However, there is a strip of conditions in between the two dynamic equilibrium lines where CO_2 would adsorb and dissociate, while CO would naturally desorb without further ado. This strip is not found on MXenes with a behavior like Mo_2N. There, the adsorption equilibrium lines locations for CO_2 and CO are reversed. However, the CO*+O* recombination to form CO_2*, a determining step prior to CO_2 desorption, is considerably inhibited, given the large recombination energy barriers ranging 1.30 to 2.83 eV, see Table 1, which leads to CO_2 dissociation having much larger rate constants than recombination for the explored temperature range, see Figure S6 of Section S5 of the SI. Consequently, CO_2 desorption is kinetically inhibited by the CO*+O* recombination, and so, the CO*+O* stability region spans up to the CO desorption equilibrium line, conditions at which CO would desorb, reachable by annealing and/or creating vacuum on the system.

Therefore, two reaction operating procedures are envisaged, either a continuous reagent CO_2 input flow with a continuous CO product output flow on the *operando* strip of Ti_2C-like MXenes, or a reagent CO_2 load up to CO*+O* saturation, followed by an annealing and/or vacuum process to remove the CO product, feasible on both Ti_2C- and Mo_2N-like MXenes. Notice that the operating type is indeed defined by the aforementioned CO_2 *vs*. CO adsorption strength balance. Whichever the case, though, one has to keep in mind that one would end up having the MXene catalyst partially covered with O* species. Such strongly attached O adatoms could act as a catalyst poison, as seen, *e.g.* on the easy formation of surface oxycarbides on parent rocksalt TMCs, where such surface oxygen is regarded as a catalyst activity-killer,[46] even if recent works revealed that oxycarbides may retain the CO_2 capture capabilities, especially on Group IV TMCs.[47]

Indeed, it appears that bare MXenes, given their high chemical activity, are well suited for the molecular dissociation catalysis, while O-terminated MXenes, featuring a much lower chemical activity, are well suited for sensing[48,49] and electrocatalytic processes.[17,19] To back up this statement, we further analyzed the CO_2 adsorption on the Ti_2C and Mo_2N limiting cases shown in Figure 5, framing the activity of the other MXenes here considered. The computed E_{ads} values are -0.18 and -0.19 eV for Ti_2C and Mo_2N, respectively, revealing a non-activated CO_2 physisorbed state, see Figure S9 and discussion in Section S7 of the SI. As seen in Figure 5, such fully O-terminated MXenes —O coverage, θ_O, of 1 monolayer (ML)— would display CCS only at very high pressures and low temperatures, far from the *operando* conditions of CO_2 breaking, succinctly signaling that CO_2 would desorb rather than dissociate, and effectively showing that O adatoms would act as a catalytic poison.

Another open question is whether the MXenes CCS and CCU capabilities are affected by lateral interactions with O adatoms in nearly fully O-covered situations. To this end, models with a θ_O = 0.67 ML have been built for Ti_2C and Mo_2N limiting cases, mimicking previous models used to study the dry reforming of methane.[45] The computed $E_{ads}^{CO_2}$ for Ti_2C and Mo_2N are reduced to -1.36 and -0.85 eV, respectively, maintaining the CCS capability at standard working conditions, see Figure 5. Furthermore, the adsorbed CO_2 still gets activated, and easily breakable into CO* and O* moieties, overcoming the low E_b^{dis} values of 0.14 and 0.01 eV, respectively; see reaction profile in Figure S10 and discussion in Section S7 of the SI. Finally, the

resulting CO product, effectively adsorbed on θ_O = 0.78 ML models, can get more easily released, featuring lower E_{ads}^{CO} values of -0.29 and -1.75 eV for Ti_2C and Mo_2N, respectively. Thus, the CCU operating modes on the studied MXenes are preserved even when having their surfaces increasingly O-covered, with equilibrium lines simply shifting towards lower temperatures and higher CO_2 or CO partial pressures, see Figure 5, but without affecting the overall view.

In any case, despite of the previous, experimental procedures exist to get rid of such surface oxygen when necessary. For instance, Persson *et al*.[15] recently showed on Ti_3C_2 MXene that surface O* could be removed through hydrogenation for 0.5 h at 8 mbar —$8 \cdot 10^2$ Pa— and 700 ºC —~973 K—, leading to the formation of water (H_2O), which desorbs from the MXene surface at these operating conditions, in accordance to lower $E_{ads}^{H_2O}$ values, ranging from -1.43 to -2.93 eV, as recently reported using the same computational approach,[50] are lower compared to present CO_2 or CO estimates, *vide supra*. Such a treatment can be applied to remove the as-generated O* species from the MXenes (0001) surfaces, thus effectively regenerating the catalyst and closing the catalytic cycle, see Figure 6. Notice, on one hand, that Persson *et al*. required such a process to eliminate surface O* prior to CO_2 capture, as does happen here, and that this regeneration of the catalyst succinctly implies that, by the end of the catalytic cycle, one is catalyzing the RWGS reaction, yet on a two-step basis, which, nevertheless, inherently allows effectively separating CO and H_2O products, which adds up for the CO subsequent utilization in the Fischer-Tropsch process.

4. Conclusions

In summary, by coupling DFT calculations and kinetic phase diagrams, we show the very easy CO_2 dissociation on a set of 18 carbide and nitride MXene catalysts. Beyond the CO formation, which can be later used in the synthesis of other compounds, such as methanol, the results show a two-step RWGS catalysis, whose mechanism differs from the previously known associative path,[51] as here the hydrogenation step is required to regenerate the catalyst. The present results also unfold the major role of the MXenes surface charge and *d*-band center in the adsorption of reactants, where the imbalance between CO_2 and CO adsorption energies defines two possible *operando* modes, either with a continuous release of CO while dosing CO_2, or a switching mode alternating CO_2 load and reaction, followed by CO release. Regardless the employed mode, the MXene

surfaces become O-covered, implying that a catalyst regenerating step is needed, combining annealing with the surface O hydrogenation, thus generating and desorbing H_2O.

The present results pose MXenes as ideal candidate materials for CCU technologies, with highly appealing possibilities in turning the CO_2 economy into a waste-to-product model, more when using H_2 from renewable sources, which would lead to a sustainable C-cycle closure.

Associated Content

Supporting Information

The following Supporting Information is available free of charge on the ACS Publications website at DOI:
Additional computational details, adsorption sites and E_{ads} of CO_2, CO, and O on each studied MXene; the used activity descriptors; the reaction profiles for each MXene, including all the E_{ads} and energy barriers involved in the process with the definition of each term; and the kinetic phase diagrams along with a description of the methodology used.

Acknowledgements

This work has been supported by the Spanish MICIUN/FEDER RTI2018-095460-B-I00 and *María de Maeztu* MDM-2017-0767 grants and, in part, by *Generalitat de Catalunya* 2017SGR13 grant, as well as by the project CICECO-Aveiro Institute of Materials, with Refs. UIDB/50011/2020 and UIDP/50011/2020, financed by national funds through the *Fundação para a Ciência e a Tecnologia* (FCT/MCTES) and co-financed by FEDER under the PT2020 Partnership Agreement. F. I. acknowledges additional support from the 2015 ICREA Academia Award for Excellence in University Research, A. M.-G. thanks to Spanish MICIUN for the *Juan de la Cierva* postdoctoral grant (IJCI-2017-31979), F. V. is thankful to *Ministerio de Economía y Competitividad* (MEC) for his *Ramón y Cajal* (RYC-2012-10129) research contract, and J. D. G. thanks project SILVIA with reference CENTRO-01-0145-FEDER-31002.

Figure 1. Side (left) and top (right) views of a MXene *p*(3×3) supercell. Dark and light blue spheres denote upmost and bottom most metal atoms, respectively, whereas yellow spheres denote X (C or N) atoms. Letters inside the light gray spheres indicate the labelling for the four relevant high-symmetry sites on the catalyst surface: bridge (B), top (T), hollow metal (H_m) and hollow carbon/nitrogen (H_x, in practice H_C or H_N).

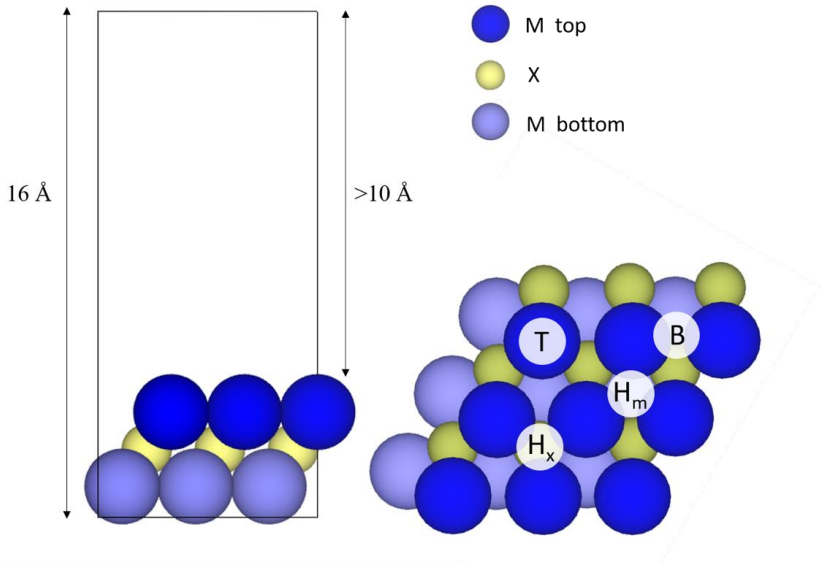

Figure 2. Linear regression of E_{ads} of most stable sites for CO_2, CO, and O adsorption on the bare $M_2X(0001)$ surfaces *versus* calculated ΔQ_m values, as listed in Table S6 of the SI. Linear regression parameters are compiled in Table S7 of the SI.

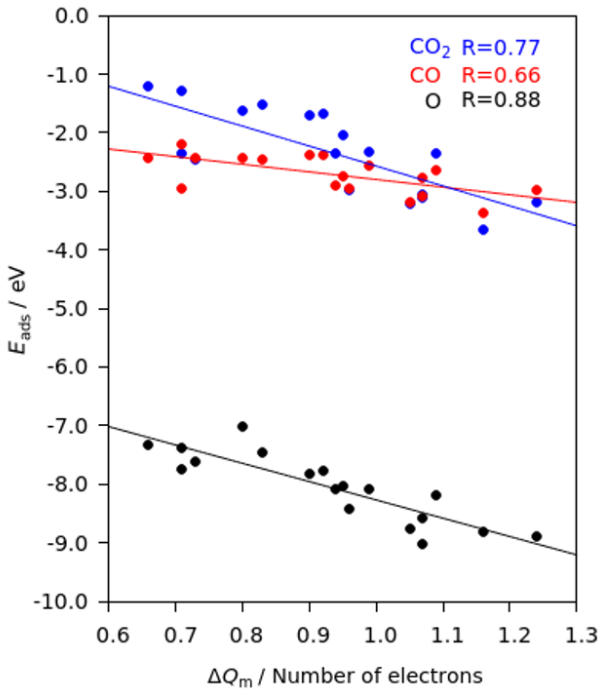

Figure 3. Linear regression of E_{ads} of most stable sites for CO_2, CO, and O on the bare $M_2X(0001)$ surfaces *versus* calculated ε_d values, as listed in Table S6 of the SI. Linear regression parameters are compiled in Table S7 of the SI.

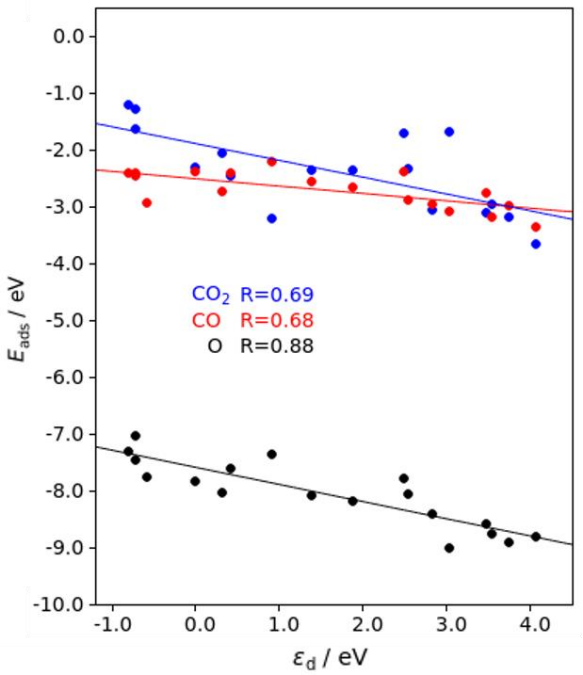

Figure 4. Reaction energy profiles for CO_2 dissociation on Ti_2C (upper panel) and Mo_2N (lower panel) basal surfaces, representing the highest and lowest CO_2-affinity situations, respectively. CO_2 adsorption and CO desorption steps are shown as initial and final stages. Lower panel images denote the different stages of adsorbed CO_2, CO_2* splitting, as-split neighbouring CO* and O* moieties, CO* or O* diffusion, CO* and O* far situations, where $E_{\mathrm{des}}^{\mathrm{CO}} = -E_{\mathrm{ads}}^{\mathrm{CO}}$. Brown spheres denote CO_2 or CO C atoms, while red, yellow, and dark and light blue denote O, X, topmost M, and bottommost M atoms, respectively.

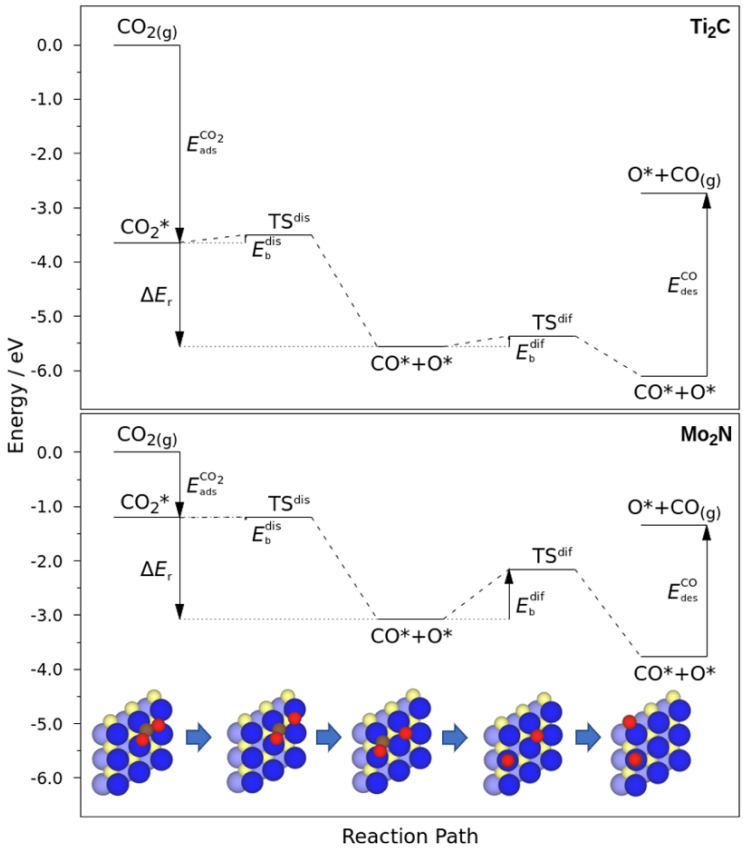

Figure 5. Kinetic phase diagrams of Ti_2C (upper panel) and Mo_2N (lower panel) as a function of CO_2 and CO partial pressures, p_{CO_2} (black left axis) and p_{CO} (red right axis), both in Pa, and temperature, *T*, in K. The standard pressure of 10^5 Pa, and temperature of 298.15 K, are shown as dashed lines. Regions of CO*+O* (grey) and O* (blue) preferences are shown shaded for the pristine θ_O coverage of 0 ML. Curved lines denote *operando* conditions where adsorption/desorption rate constants are at equilibrium, either for CO_2 (black) or CO (red). These are given either at θ_O = 0 ML, at a full O-coverage situation, θ_O = 1.0 ML, or at a nearly fully O-covered situation, θ_O = 0.67 and 0.78 ML for CO_2 and CO, respectively.

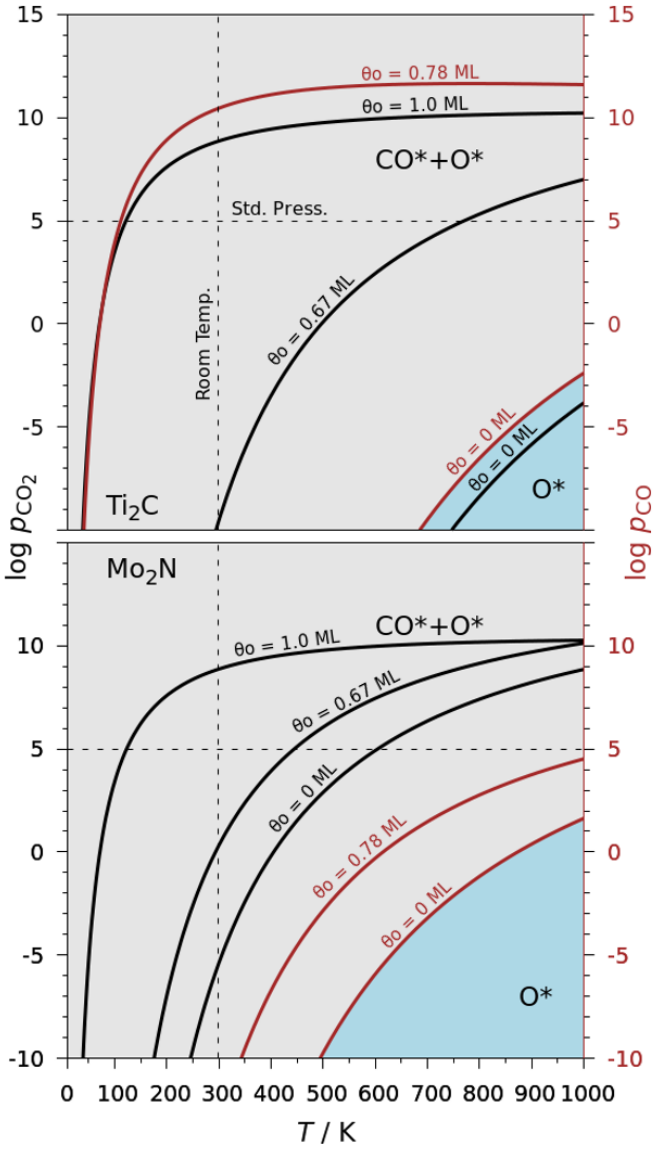

Figure 6. Scheme of the steps carried out for the RWGS reaction, including a) CO_2 adsorption, b) CO_2 dissociation, c) CO desorption, d) hydrogenation of the surface O* species and water formation, and e) H_2O desorption, closing the catalytic cycle.

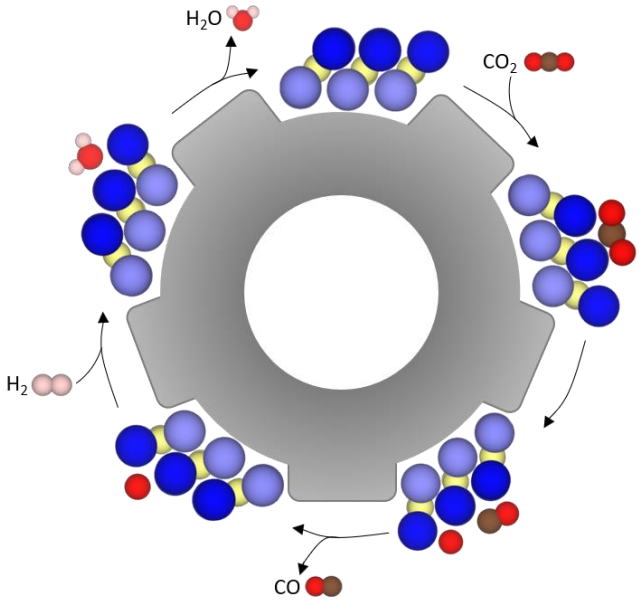

Table 1. Summary of ΔE_r, E_b^{dis}, and E_b^{rec} values, including ZPE, for CO_2 dissociation process on the most stable adsorption site (upper row) and second most stable site (lower row) for each studied $M_2X(0001)$ surface. All values are given in eV.

	M	**M_2N**			**M_2C**		
		ΔE_r	**E_b^{dis}**	**E_b^{rec}**	**ΔE_r**	**E_b^{dis}**	**E_b^{rec}**
d^2	Ti	-2.33 / $C_mO_xO_x$	0.05	2.38	-1.92 / $C_xO_mO_m$	0.14	2.06
		-1.95 /$C_xO_mO_m$	0.05	2.03	-2.18 / $C_mO_xO_x$	0.08	2.29
	Zr	-2.45 /$C_mO_xO_x$	0.03	2.48	-1.66 /$C_xO_mO_m$	0.12	1.78
		—	—	—	-2.12 / $C_mO_xO_x$	0.10	2.26
	Hf	-2.75 /$C_mO_xO_x$	~0	2.75	-2.10 /$C_xO_mO_m$	0.03	2.12
		—	—	—	-2.45 /$C_mO_xO_x$	0.03	2.53
d^3	V	-2.23 / C_b	0.09	2.32	-2.14 / $C_xO_mO_m$	0.01	2.13
		-2.26 /C_mO_b	0.10	2.39	-2.15 / C_mO_b	~0	2.16
	Nb	-2.21 / C_b	0.28	2.49	-2.48 / C_mO_b	0.11	2.59
		-2.34 / C_mO_b	0.26	2.65	—	—	—
	Ta	-1.95 / $C_mO_xO_x$	0.52	2.47	-2.32 / C_mO_b	0.51	2.83
		-0.88 / $C_xO_mO_m$	0.38	1.30	—	—	—
d^4	Cr	-1.23 / $C_bO_bO_b$	0.49	1.72	-1.66 / $C_bO_bO_b$	0.24	1.90
	Mo	-1.87 /$C_bO_bO_b$	~0	1.85	-1.52 / C_mO_b	0.28	1.80
		-2.01 / C_b	~0	2.06	—	—	—
	W	-1.10 / $C_mO_mO_b$	0.35	1.45	-1.95 / $C_xO_mO_m$	0.54	2.50

References

(1) Intergovernmental Panel on Climate Change, *Climate Change 2014: Synthesis Report*; IPCC, 2015.

(2) Leung, D. Y. C.; Caramanna, G.; Maroto-Valer, M. M. An Overview of Current Status of Carbon Dioxide Capture and Storage Technologies. *Renew. Sust. Energ. Rev.* **2014**, *39*, 426-443.

(3) Boot-Handford, M. E.; Abanades, J. C; Anthony, E. J.; Blunt, M. J.; Brandani, S.; MacDowell, N.; Fernández, J. R.; Ferrari, M.-C.; Gross, R.; Hallett, J. P.; Haszeldine, R. S.; Heptonstall, P.; Lyngfelt, A.; Makuch, Z.; Mangano, E.; Porter, R. T. J.; Pourkashanian, M.; Rochelle, G. T.; Shah, N.; Yao, J. G.; Fennell, P. S. Carbon Capture and Storage Update. *Energy Environ. Sci.* **2014**, *7*, 130-189.

(4) D'Alessandro, D. M.; Smit, B.; Long, J. R. Carbon Dioxide Capture: Prospects for New Materials. *Angew. Chem. Int. Ed.* **2010**, *49*, 6058-6082.

(5) Hansen, J.; Sato, M.; Kharecha, P.; von Schuckmann, K.; Beerling, D. J.; Cao, J.; Marcott, S.; Masson-Delmotte, V.; Prather, M. J.; Rohling, E. J.; Shakun, J.; Smith, P.; Lacis, A.; Russell, G.; Ruedy, R. Young People's Burden: Requirement of Negative CO_2 Emissions. *Earth Syst. Dynam.* **2017**, *8*, 577-616.

(6) Kondratenko, E. V.; Mul, G.; Baltrusaitis, J.; Larrazabal, G. O.; Pérez-Ramírez, J. Status and Perspectives of CO_2 Conversion into Fuels and Chemicals by Catalytic, Photocatalytic and Electrocatalytic Processes. *Energy Environ. Sci.* **2013**, *6*, 3112-3135.

(7) Markewitz, P.; Kuckshinrichs, W.; Leitner, W.; Linssen, J.; Zapp, P.; Bongartz, R.; Schreiber, A.; Müller, T. E. Worldwide Innovations in the Development of Carbon Capture Technologies and the Utilization of CO_2. *Energy Environ. Sci.* **2012**, *5*, 7281-7305.

(8) Yu, K. M. K.; Curcic, I.; Gabriel, J.; Tsang, S. C. E. Recent Advances in CO_2 Capture and Utilization. *ChemSusChem* **2008**, *1*, 893-899.

(9) Aricò, A. S.; Srinivasan, S.; Antonucci, V. DMFCs: From Fundamental Aspects to Technology Development. *Fuel Cells* **2001**, *1*, 133-161.

(10) Schulz, H. Short History and Present of Fischer-Tropsch Synthesis. *Appl. Catal. A* **1999**, *186*, 3-12.

(11) Fajín, J. L. C.; Cordeiro, M. N. D. S.; Gomes, J. R. B. Fischer-Tropsch Synthesis on Multicomponent Catalysts: What Can We Learn from Computer Simulations? *Catalysts* **2015**, *5*, 3-17.

(12) Naguib, M.; Kurtoglu, M.; Presser, V.; Lu, J.; Niu, J.; Heon, M.; Hultman, L.; Gogotsi, Y.; Barsoum, M. W. Two-Dimensional Nanocrystals by Exfoliation of Ti_3AlC_2. *Adv. Mater.* **2011**, *23*, 4248-4253.

(13) Morales-García, Á.; Fernández-Fernández, A.; Viñes, F.; Illas, F. CO_2 Abatement Using Two-Dimensional MXenes Carbides. *J. Mater. Chem. A* **2018**, *6*, 3381-3385.

(14) Morales-Salvador, R.; Morales-García, Á.; Viñes, F.; Illas, F. Two-Dimensional Nitrides as Highly Potential Candidates for CO_2 Capture and Activation. *Phys. Chem. Chem. Phys.* **2018**, *20*, 17117-17124.

(15) Persson, I.; Halim, J.; Lind, H.; Hansen, T. W.; Wagner, J. B.; Näslund, L.-Å.; Darakchieva, V.; Palisaitis, J.; Rosen, J.; Persson, P. O. Å. 2D Transition Metal Carbides (MXenes) for Carbon Capture. *Adv. Mater.* **2019**, *31*, 1805472.

(16) Handoko, A. D.; Steinmann, S. N.; Seh, Z. W. Theory-Guided Materials Design: Two-Dimensional MXenes in Electro- and Photocatalysis. *Nanoscale Horiz.* **2019**, *4*, 809-827.

(17) Handoko, A. D.; Chen, H.; Lum, Y.; Zhang, Q.; Anasori, B.; Seh, Z. W. Two-Dimensional Titanium and Molybdenum Carbide MXenes as Electrocatalysts for CO_2 Reduction. *iScience* **2020**, *23*, 101181.

(18) Chen, H.; Handoko, A. D.; Xiao, J.; Feng, X.; Fan, Y.; Wang, T.; Legut, D.; Seh, Z. W.; Zhang, Q. Catalytic Effect on CO_2 Electroreduction by Hydroxyl-Terminated Two-Dimensional MXenes. Catalytic Effect on CO_2 Electroreduction by Hydroxyl-Terminated Two-Dimensional MXenes. *ACS Appl. Mater. Interfaces* **2019**, *11*, 36571−36579.

(19) Handoko, A. D.; Khoo, K. H.; Tan, T. L.; Jin, H.; Seh, Z. W. Establishing new Scaling Relations on Two-Dimensional MXenes for CO_2 Electroreduction. *J. Mater. Chem. A* **2018**, *6*, 21885−21890.

(20) Chen, H.; Handoko, A. D.; Wang, T.; Qu, J.; Xiao, J.; Liu, X.; Legut, D.; Seh, Z. W.; Zhang, Q. Defect-Enhanced CO_2 Reduction Catalytic Performance in O-Terminated MXenes. *ChemSusChem* **2020**, *13*, 5690–5698.

(21) Lim, K. R. G.; Handoko, A. D.; Nemani, S. K.; Wyatt, B.; Jiang, H.-Y.; Tang, J.; Anasori, B.; Seh, Z. W. Rational Design of Two-Dimensional Transition Metal Carbide/Nitride (MXene) Hybrids and Nanocomposites for Catalytic Energy Storage and Conversion. *ACS Nano* **2020**, *14*, 10834–10864.

(22) Kamysbayev, V.; Filatov, A. S.; Hu, H.; Rui, X.; Lagunas, F.; Wang, D.; Klie, R. F.; Talapin, D. V. Covalent Surface Modifications and Superconductivity of Two-Dimensional Metal Carbide MXenes. *Science* **2020**, *369*, 979-983.

(23) Kresse, G.; Joubert, D. From Ultrasoft Pseudopotentials to the Projector Augmented-Wave Method. *Phys. Rev. B* **1999**, *59*, 1758.

(24) Perdew, J. P.; Burke, K.; Ernzerhof, M. Generalized Gradient Approximation Made Simple. *Phys. Rev. Lett.* **1996**, 77, 3865.

(25) Grimme, S.; Antony, J.; Ehrlich, S.; Krieg, H. A Consistent and Accurate *Ab Initio* Parametrization of Density Functional Dispersion Correction (DFT-D) for the 94 Elements H-Pu. *J. Chem. Phys.* **2010**, *132*, 154104.

(26) Liu, X.; Kunkel, C.; Ramírez de la Piscina, P.; Homs, N.; Viñes, F.; Illas, F. Effective and Highly Selective CO Generation from CO_2 Using a Polycrystalline α-Mo_2C. *ACS Catal.* **2017**, *7*, 4323-4335.

(27) Kunkel, C.; Viñes, F.; Illas, F. Transition Metal Carbides as Novel Materials for CO_2 Capture, Storage, and Activation. *Energy Environ. Sci.* **2016**, *9*, 141-144.

(28) Blöch, P. E. Projector Augmented-Wave method. *Phys. Rev. B* **1994**, *50*, 17953.

(29) Monkhorst, H. J.; Pack, J. D. Special Points for Brillouin-Zone Integrations. *Phys. Rev. B* **1976**, *13*, 5188.

(30) Henkelman, G.; Uberuaga, B. P.; Jónsson, H. A Climbing Image Nudged Elastic Band Method for Finding Saddle Points and Minimum Energy Paths. *J. Chem. Phys.* **2000**, *113*, 9901.

(31) Maragakis, P.; Andreev, S.A.; Brumer, Y.; Reichman, D. R.; Kaxiras, E. Adaptive Nudged Elastic Band Approach for Transition State Calculation. *J. Chem. Phys.* **2002**, *117*, 4651.

(32) Henkelman, G.; Jónsson, H. A Dimer Method for Finding Saddle Points on High Dimensional Potential Surfaces Using Only First Derivatives. *J. Chem. Phys.* **1999**, *111*, 7010.

(33) Heyden, A.; Bell, A. T.; Keil, F. J. Efficient Methods for Finding Transition States in Chemical Reactions: Comparison of Improved Dimer Method and Partitioned Function Optimized Method. *J. Chem. Phys.* **2005**, *123*, 224101.

(34) Prats, H.; McAloone, H.; Viñes, F.; Illas, F. Ultra-High Selectivity Biogas Upgrading Through Porous MXenes. *J. Mater. Chem. A* **2020**, *8*, 12296-12300.

(35) Naguib, M.; Mashtalir, O.; Carle, J.; Presser, V.; Lu, J.; Hultman, L.; Gogotsi, Y.; Barsoum, M. W. Two-Dimensional Transition Metal Carbides. *ACS Nano* **2012**, *6*, 1322-1331.

(36) Hope, M. A.; Forse, A. C.; Griffith, K. J.; Lukatskaya, M. R.; Ghidiu, M.; Gogotsi, Y.; Grey, C. P. NMR Reveals the Surface Functionalisation of Ti_3C_2 MXene. *Phys. Chem. Chem. Phys.* **2016**, *18*, 5099-5102.

(37) Ibragimova, R.; Puska, M. J.; Komsa, H.-P. pH-Dependent Distribution of Functional Groups on Titanium-Based MXenes. *ACS Nano* **2019**, *13*, 9171-9181.

(38) Gouveia, J. D.; Viñes, F.; Illas, F.; Gomes, J. R. B. MXenes Atomic Layer Stacking Phase Transitions and their Chemical Activity Consequences. *Phys. Rev. Mater.* **2020**, *4*, 054003.

(39) Porosoff, M. D.; Kattel, S.; Li, W.; Liu, P.; Chen, J. G. Identifying Trends and Descriptors for Selective CO_2 Conversion to CO over Transition Metal Carbides. *Chem. Commun.* **2015**, *51*, 6988-6991.

(40) Morales-García, Á.; Mayans-Llorach, M.; Viñes, F.; Illas, F. Thickness Biased Capture of CO_2 on Carbides MXenes. *Phys. Chem. Chem. Phys.* **2019**, *21*, 23136-23142.

(41) Henkelman, G.; Arnaldsson, A.; Jónsson, H. A Fast and Robust Algorithm for Bader Decomposition of Charge Density. *Comput. Mater. Sci.* **2006**, *36*, 354-360.

(42) Bader, R. F. W. *Atoms in Molecules: A Quantum Theory*. Oxford University Press, **1994**.

(43) Hammer, B.; Nørskov, J. K. Electronic Factors Determining the Reactivity of Metal Surfaces. *Surf. Sci.* **1995**, *343*, 211-220.

(44) Muttaqien, F.; Hamamoto, Y.; Inagaki, K.; Morikawa, Y. Dissociative Adsorption of CO_2 on Flat, Stepped, and Kinked Cu Surfaces. *J. Chem. Phys.* **2014**, *141*, 034702.

(45) Kurlov, A.; Deeva, E. B.; Abdala, P. M.; Lebedev, D.; Tsoukalou, A.; Comas-Vives, A.; Fedorov, A.; Müller, C. R. Exploiting Two-Dimensional Morphology of Molybdenum Oxycarbide to Enable Efficient Catalytic Dry Reforming of Methane. *Nat. Commun.* **2020**, *11*, 4920.

(46) Hwu, H. H.; Chen, J. G. Surface Chemistry of Transition Metal Carbides. *Chem. Rev.* **2005**, *105*, 185-212.

(47) Kunkel, C.; Viñes, F.; Illas, F. Surface Activity of Early Transition-Metal Oxycarbides: CO_2 Adsorption Case Study. *J. Phys. Chem. C* **2019,** *123*, 3664-3671.

(48) Gouveia, J. D.; Novell-Leruth, G.; Viñes, F.; Illas, F.; Gomes, J. R. B. The Ti_2CO_2 MXene as a Nucleobase 2D Sensor: A First-Principles Study. *Appl. Surf. Sci.* **2021**, *544*, 148946.

(49) Gouveia, J. D.; Novell-Leruth, G.; Viñes, F.; Illas, F.; Gomes, J. R. B. First-Principles Calculations on the Adsorption Behavior of Amino Acids on a Titanium Carbide MXene. *ACS Appl. Bio Mater.* **2020**, *3*, 5913-5921.

(50) Gouveia, J. D.; Morales-García, Á.; Viñes, F.; Illas, F.; Gomes, J. R. B. MXenes as Promising Catalysts for Water Dissociation. *Appl. Catal. B - Environ.* **2020**, *260*, 118191.

(51) Posada-Pérez, S.; Ramírez, P. J.; Gutiérrez, R. A.; Stacchiola, D. J.; Viñes, F.; Liu, P.; Illas, F.; Rodriguez, J. A. The Conversion of CO_2 to Methanol on Orthorombic β-Mo_2C and Cu/ β-Mo_2C Catalysts: Mechanism for Admetal Induced Change in the Selectivity and Activity. *Catal. Sci. Technol.* **2016**, *6*, 6766-6777.

Table of Contents